Fabrication of 3D multi-layered ZnCo-LDH as a heterogeneous photoactivator of peroxymonosulfate for efficient degradation of rhodamine B

Shu Zhou, Guoqing Zhao, YinKe Wang, Lukai Liu, Feipeng Jiao*

School of Chemistry and Chemical Engineering, Central South University, Changsha 410083, China, email: jiaofp@csu.edu.cn (F. Jiao)

ABSTRACT

Peroxymonosulfate (PMS)-based advanced oxidation processes have been widely concerned because of their efficient treatment and wide applicability for the removal of various organic pollutants. In this study, ZnCo layered double hydroxide (ZnCo-LDH) were prepared by the hydrothermal method, analyzed by several characterization methods, and tested as a heterogeneous photoactivator to activate PMS for the removal of refractory organic dyes. The experimental results showed that 3D multi-layered ZnCo-LDH (1:1) catalyst can activate PMS to achieve the main degradation of 10 mg L^{-1} rhodamine B (RhB) under dark within 40 min. Moreover, the RhB can be completely degraded within 30 min by supplying the additional visible light under the same conditions. It can be seen that all degraded reaction processes were corresponded with the pseudo-first-order kinetic model, and the highest rate of RhB removal is 0.1303 min^{-1} in visible light. The effect of various conditions including the reaction system, inorganic anions, and initial pH on the RhB degradation was analyzed in detail. The ZnCo-LDH (1:1) catalyst can still keep high catalytic activity to PMS and achieved more than 95% degradation efficiency even after continual four recycles. In addition, the reaction mechanism indicated that hydroxyl radical ($^{\bullet}OH$) and sulfate radical ($SO_4^{\bullet-}$) can effectively oxidize RhB by the single activation of ZnCo-LDH catalyst, and this reaction process can also be enhanced under visible light irradiation. Briefly, the heterogeneous PMS-AOPs synergistic techniques could be a promising work for the integrated control of environmental pollution.

Keywords: ZnCo-LDH; Peroxymonosulfate; Activation; Degradation; Rhodamine B

1. Introduction

Organic dye is an important chemical product, which has been widely applied in all aspects of daily life including textiles, plastic ware, and ceramics [1]. It is reported that a considerable part of dyes will finally enter into water environment, which results in significant reduction of water transparency and biological oxygen demand [2]. Afterwards, pollutant problems caused by organic dyes have attracted extensive attention due to its serious hazards to natural environment and human health [3]. Therefore, it

is necessary that a kind of green and efficient approach is developed to remove the organic dyes from the industrial wastewater. In recent decades, several approaches are used to remove dye contaminants, including ultrasound oxidation, biological oxidation, physical adsorption, and membrane separation techniques [4–7]. However, most of the above approaches can only separate the contained pollutants from wastewater and fail to decompose into the small non-toxic molecules. In contrast, some refractory dyes can be effectively oxidized and degraded by using advanced oxidation processes (AOPs).

* Corresponding author.

At present, AOPs technologies have brought about widespread attention because of their excellent oxidation capacity, high degradation rate, and wide applicability for the degradation of various organic pollutants [8,9]. Commonly, PMS-based AOPs technologies are used to degrade all kinds of dyes by oxidation of $^{\bullet}OH$ and $SO_4^{\bullet-}$ radicals which are derived from PMS through special activator such as ultraviolet irradiation, active carbon, and transition metal ions [10–12]. Among them, it was discovered that the Co^{2+}/PMS system showed the excellent performance to produce many active species including $^{\bullet}OH$ and $SO_4^{\bullet-}$ radicals [13]. For example, Xie et al. [14] prepared the porous Co-doped $g-C_3N_4$ to improve activation of PMS for the degradation of chlorophenols. Furthermore, Zeng et al. [15] synthesized the yolk-shell $Co_3O_4@MOFs$ catalysts to activate PMS effectively for completed degradation of 4-chlorophenol as compared to only 59.6% for pure Co_3O_4 nanoparticles under the same conditions. In addition, above some researches indicated that heterogeneous cobalt-based catalysts with specific structure can improve activated ability of catalyst as well as avoid the second pollution of metal ions leaching. Hence, it is urgent to develop the heterogeneous Co/PMS systems which have high efficiency and good stability for the effective treatment of organic dye wastewater.

Layered double hydroxides (LDHs) as typical anionic clay is commonly called as the hydrotalcite-like compounds. It has a special layer structure including positively charged brucite-like layers of main body layer board and compensating anions between the layers [16,17]. Commonly, it can be described by this typical formula: $[M_{1-x}^{2+}M_x^{3+}(OH)_2]^{x+}(A^{n-})_{x/n} \cdot mH_2O$, in which M^{2+} and M^{3+} represent divalent and trivalent cation, respectively, and A^{n-} is the interlayer anion of charge n, x denotes the molar ratio of $M^{3+}/(M^{2+} + M^{3+})$, and m is the molar amount of crystal water [18–21]. As a typical heterogeneous catalyst, LDHs have been widely applied in the catalytic and adsorption fields owing to its unique advantages such as simple synthesis, adjustable structure, and large specific surface area [22,23]. For instance, Zhao et al. [24] synthesized a CoMn-LDH as an effective heterogeneous catalyst to activate peroxymonosulfate (PMS) for the degradation of AOG dyes [24]. Besides, it is reported that ZnAlFe-LDH has good photocatalytical performance for the photocatalytic degradation of 2,4-dichlorophenoxyacetic acid [25]. Therefore, we propose to design 3D multi-layered ZnCo-LDH as cobalt-based catalyst which has large specific area and special lamellar structure to expose more active sites for the effective activation of PMS, and the combination of LDH catalyst with PMS can also further enhance this reaction process under visible light irradiation. As far as we are concerned, there are almost no reports about advanced techniques of synergistic heterogeneous Co-based catalyst/PMS photosystem.

In this work, the ZnCo-LDH catalyst was synthesized via the hydrothermal method. Its morphological and structural features were clearly investigated by several characterizations, and then the degradation properties of RhB were explored under visible light irradiation. The important influence factors including pH values and the inorganic anions were explored by the condition experiments. In addition, the relevant reaction mechanism of radical intermediates was proposed in the degraded processes of RhB.

Finally, the stability and reusability of the ZnCo-LDH catalyst were tested by four recycle tests. This work might provide an efficient green and feasible synergistic technique to treat the dye pollutants from industrial wastewater.

2. Materials and methods

2.1. Chemicals

All chemicals were analytical-reagent grades and used as received of reagent or higher purity, and all solutions were prepared with the ultrapure water in the whole experimental processes. PMS ($KHSO_5 \cdot 0.5KHSO_4 \cdot 0.5K_2SO_4$, 95.0%) was purchased by Saen Technology Co., Ltd., (Shanghai, China). Rhodamine B dye (RhB, $C_{28}H_{31}ClN_2O_3$) was provided by Tianjin Kemiou Chemical Reagent Co., Ltd. Zinc nitrate hexahydrate ($Zn(NO_3)_2 \cdot 6H_2O$), aluminum nitrate nonahydrate ($Al(NO_3)_3 \cdot 9H_2O$), cobalt nitrate hexahydrate ($Co(NO_3)_2 \cdot 6H_2O$), urea ($CO(NH_2)_2$), ethanol (CH_3CH_2OH), *tert*-butyl alcohol (TBA) were purchased from Sinopharm Chemical Reagent Co., Ltd., (Shanghai, China).

2.2. Preparation of catalyst

3D multi-layered ZnCo-LDH was prepared by the hydrothermal method. Firstly, an equal amount of $Zn(NO_3)_2 \cdot 6H_2O$ and $Co(NO_3)_2 \cdot 6H_2O$ (Zn/Co molar ratio 1:1) were added into 80 mL deionized water with vigorous stirring. After that, a certain amount of urea as the precipitant was added in this salt solution with magnetic stirring, and then the mixed solution was transferred into 100 mL Teflon-lined steel reactor at 150°C for 12 h. Finally, the precipitate was obtained via centrifuging and washing with ethanol and deionized water for several times, and dried at 60°C in the oven. The obtained material was denoted as ZnCo-LDH (1:1). Besides, other LDH materials were similarly prepared with the different addition of cobalt source and called as ZnCo-LDH (2:1), ZnCo-LDH (3:1), and ZnAl-LDH, respectively.

2.3. Characterization

The crystalline phases analysis of the as-prepared samples was obtained by using the X-ray diffractometer (XRD, D8 Advanced, Bruker Co., Germany) at the condition of Cu Kα radiation (λ = 1.5406 Å, 40 mA, and 40 KV), and the corresponding data were completely recorded at a 2θ range of 10°–80° with a scanning rate of 8°/min. The morphological structure and elemental composition were obtained by using scanning electron microscopy (SEM, TESCAN MIRA3 LMU) and energy-dispersive X-ray spectroscopy (EDX) at an accelerating voltage of 10 kV. The Fourier transform infrared (FT-IR) spectra can be used to analyze relevant functional groups at the range of 4,000–500 cm^{-1} by using an AVATAR 360 spectrometer (Nicolet Instrument Corp., America). The specific surface area and porosity of the samples were determined by using Brunauer–Emmett–Teller (BET) under the following parameters: 77 K, 6 h outgas, and 300°C in advance. Besides, the Barrett–Joyner–Halenda (BJH) method was carried out to study the pore volume and diameter. X-ray photoelectron spectroscopy (XPS)

measurement was taken by using the ULVAC-PHI spectrometer (Thermo Fisher Scientific, UK) with non-monochromatic Al Ka X-rays beam (1,486.6 eV).

2.4. Catalytic activity test

The degradation experiment of RhB was carried out in a test tube containing 50 mL of simulated pollutant solution under the Xe lamp (500 W) with a 400 nm cut filter. In a typical degradation of RhB, 25 mg ZnCo-LDH catalysts were added into RhB dye solution (10 mg L^{-1}) with a constant stirring to obtain uniform dispersion. The adsorption–desorption equilibrium has been built after stirring of 30 min in dark. Then, the reaction solution was exposed under visible light to start the reaction after the addition of 15 mg PMS. After a time interval of 8 min, 3 mL sample was collected and filtered to remove the catalyst particles. The concentration variation of RhB was obtained by testing this sample liquid by using a UV-vis spectrophotometer (UV-9600) at the characteristic absorption peak of 554 nm. Due to the very low adsorption of ZnCo-LDH catalysts for RhB, the effects of adsorption on whole degradation experiments can be ignored, and the corresponding degradation efficiencies of RhB can be described as this general formula: DE% = $(C_0 - C_t)/C_0$, where C_t is the real-time concentration and C_0 is the initial concentration.

3. Results and discussion

3.1. Structural characterization

The XRD pattern of ZnCo-LDH samples is presented in Fig. 1a. It is discovered that the characteristic diffraction peaks were about 25°, 33°, 38°, 43°, 47°, and 53° which accord with the lattice plane of (006), (100), (012), (015), (018), and (102) planes according to the previous work [26]. The sharp diffraction peaks showed its high crystallinity in these samples. Besides, the ZnCo-LDH (1:1) exhibited a few clear diffraction peaks of the typical brucite-like layers with the

increase of cobalt source. The above results indicated that the high purity of hierarchical ZnCo-LDH was successful synthesized by the hydrothermal method, and it does not contain any other impurity peaks.

The FT-IR spectra of ZnCo-LDH samples are shown in Fig. 1b. There is a broad absorption peak at about 3,428 cm^{-1}, which revealed the stretching vibration of the O–H groups from the hydroxide layers and water molecules form the interlayer [27]. Besides, the strong peak at nearly 1,653 cm^{-1} revealed the existence of water molecules with the bending vibration. The peak at around 1,380 and 2,360 cm^{-1} can be associated with the C–O stretching of interlayer carbonate ions and the weak absorption of carbon dioxide, respectively [28]. Notably, a large of peaks existed in the range of about 500–1,000 cm^{-1}, which can be ascribed to the stretching vibrations of metallic bond (Zn–OH and Co–OH) [29]. It can be seen that the three samples have similar peak shape and peak location which will not be affected by metal contents.

The SEM images were used to analyze the morphological structure of samples. As shown in Fig. 2a, the ZnCo-LDH (1:1) has homogeneous cubical morphology structure with a relatively wide size distribution and good dispersion. Commonly, the construction of ZnCo-LDH has many main body layers which are consisted with octahedral units with central metal cations, and each vertex angle existed the hydroxyl ions. In order to balance the extra positive charge of main body layers, the carbonate ions as compensating anions were intercalated between the interlayer regions. The 3D multi-layered ZnCo-LDH showed the construction of octahedron unit which has lamellar structure with the large surface area. Besides, it can support layered structure with more active site, which is beneficial to the adsorption of targeted dyes and enhancement of degradation process. In Fig. 2b, the EDX elemental spectrum illustrates that the elements including Zn, Co, and O were contained in ZnCo-LDH samples without other impurities.

The adsorption of ZnCo-LDH (1:1) was associated with the pore structure as well as specific surface area of
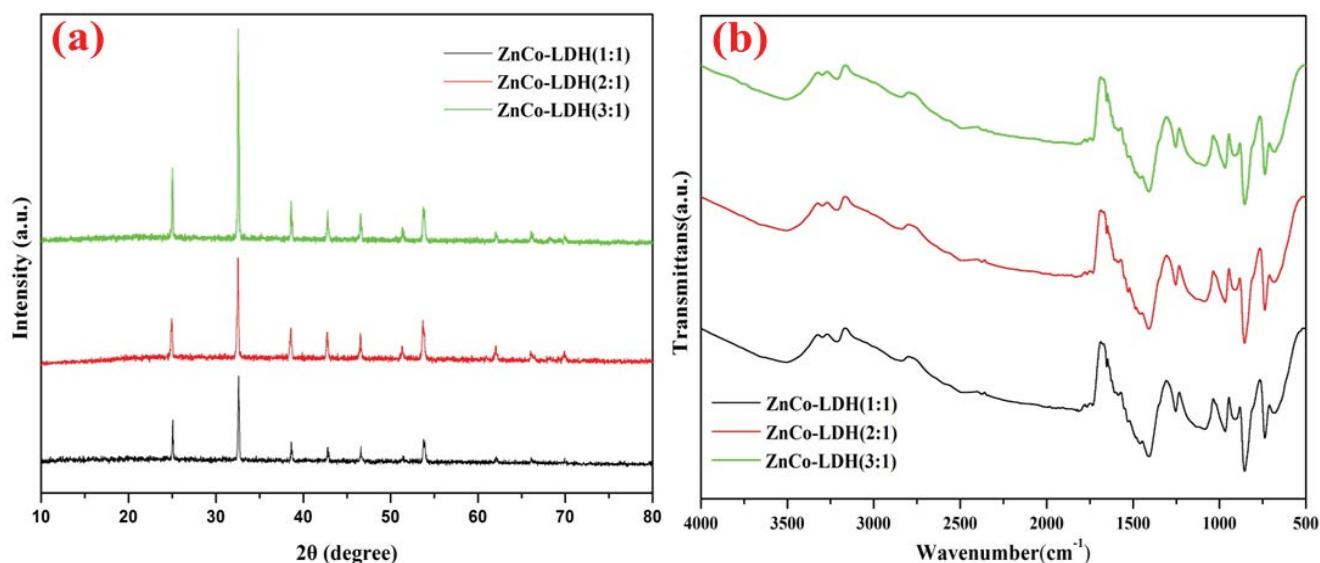
Fig. 1. (a) XRD pattern and (b) FT-IR spectra of different ZnCo-LDH samples.
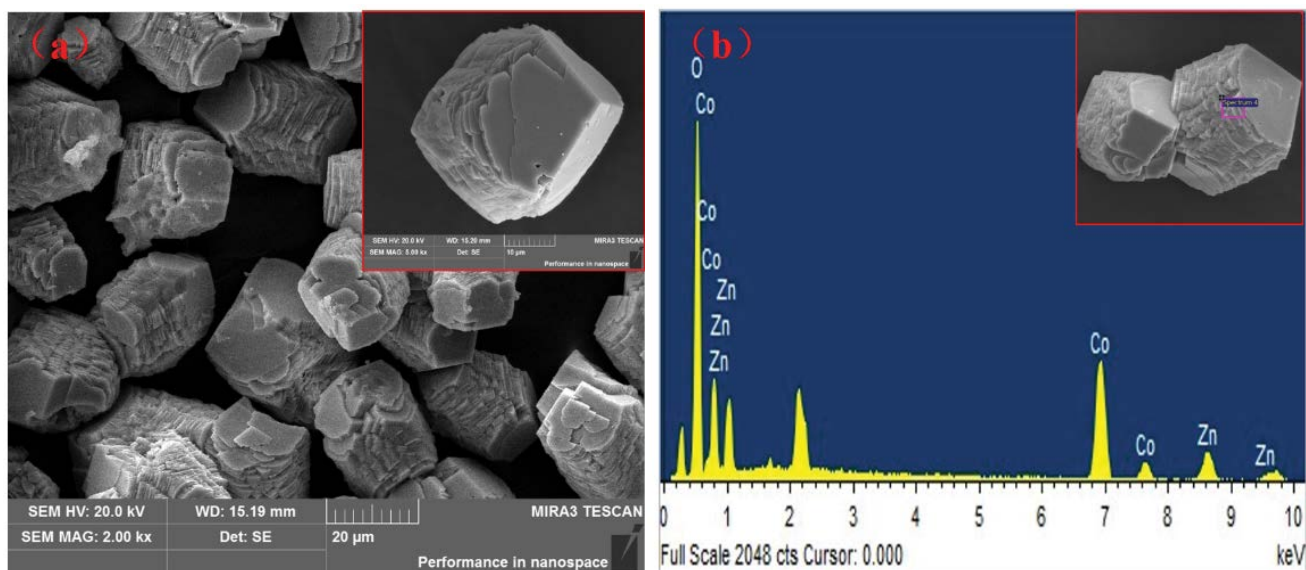
Fig. 2. (a) SEM image and (b) EDX map of ZnCo-LDH (1:1).

as-prepared catalyst. As shown in Figs. 3a and b, the N_2 adsorption–desorption isotherms curve and the relevant pore-size distribution curve were obtained by the test and analysis. Based on the descriptions of the International Union of Pure and Applied Chemistry (IUPAC), ZnCo-LDH (1:1) presented an obvious IV isotherm fitted to the H3 type hysteresis loop, which was well accorded with the typical characteristics of microporous structures. From Fig. 3a, a hysteresis loop and abrupt leap are observed in this region (P/P_0 = 0.2–1.0), which indicated that the interconnected channels can be existed in ZnCo-LDH (1:1) catalyst. Fig. 3b displays the pore-size distribution of ZnCo-LDH (1:1), and its pore diameters are mostly presented at the range of 2–10 nm which furthermore confirmed the existence of mesopores. In addition, the adsorption kinetics parameters

were obtained, including the surface area (4.853 m² g⁻¹), pore volume (0.006 cm³ g⁻¹), and pore diameter (2.173 nm), respectively. Therefore, it can be concluded from above results that 3D multi-layered ZnCo-LDH (1:1) catalyst has the microporous structures with many active sites, thus improving the degradation efficiency of the organic pollutants.

XPS test results was employed to analyze the element valence states of the ZnCo-LDH (1:1) in Fig. 4. It can be seen that the main elements of the survey XPS spectrum included Zn, Co, O, and C in Fig. 4a. More notably, the peak of C 1s at 285.1 eV are owing to external carbon contamination from the signal of carbon of the apparatus. The results of Fig. 4b indicate that the peaks at 1,045.2 and 1,022.1 eV could be assigned to the binding energies of Zn $2p_{1/2}$ and Zn $2p_{3/2}$, respectively. In Fig. 4c, the two binding energies peaks at
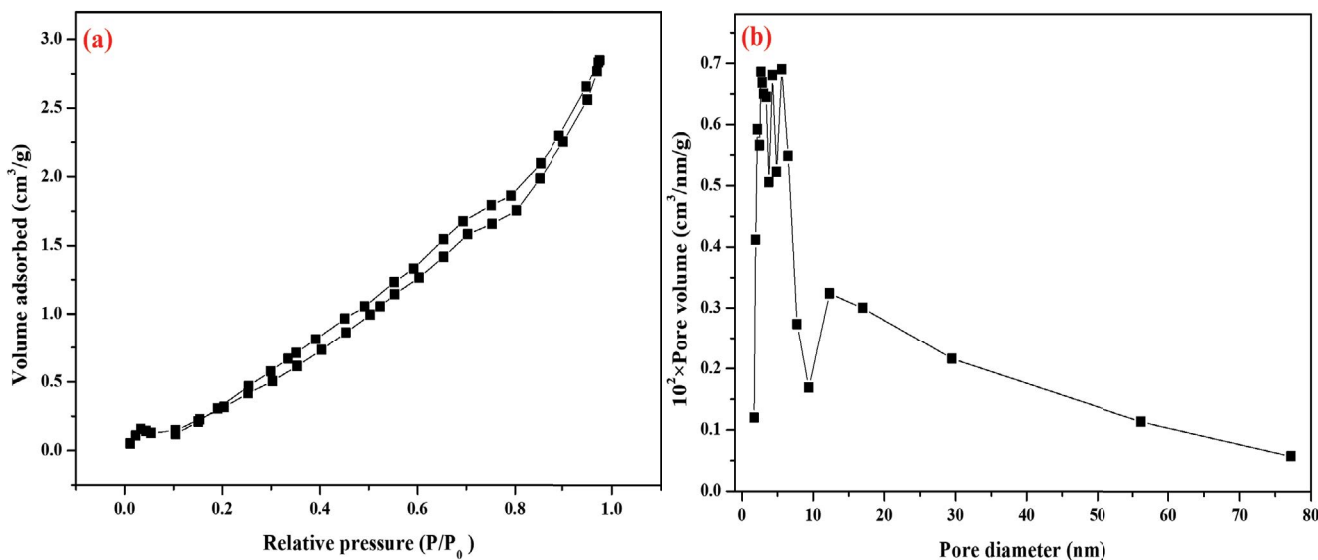
Fig. 3. (a) N_2 adsorption–desorption isotherms and (b) pore size distributions of ZnCo-LDH (1:1).
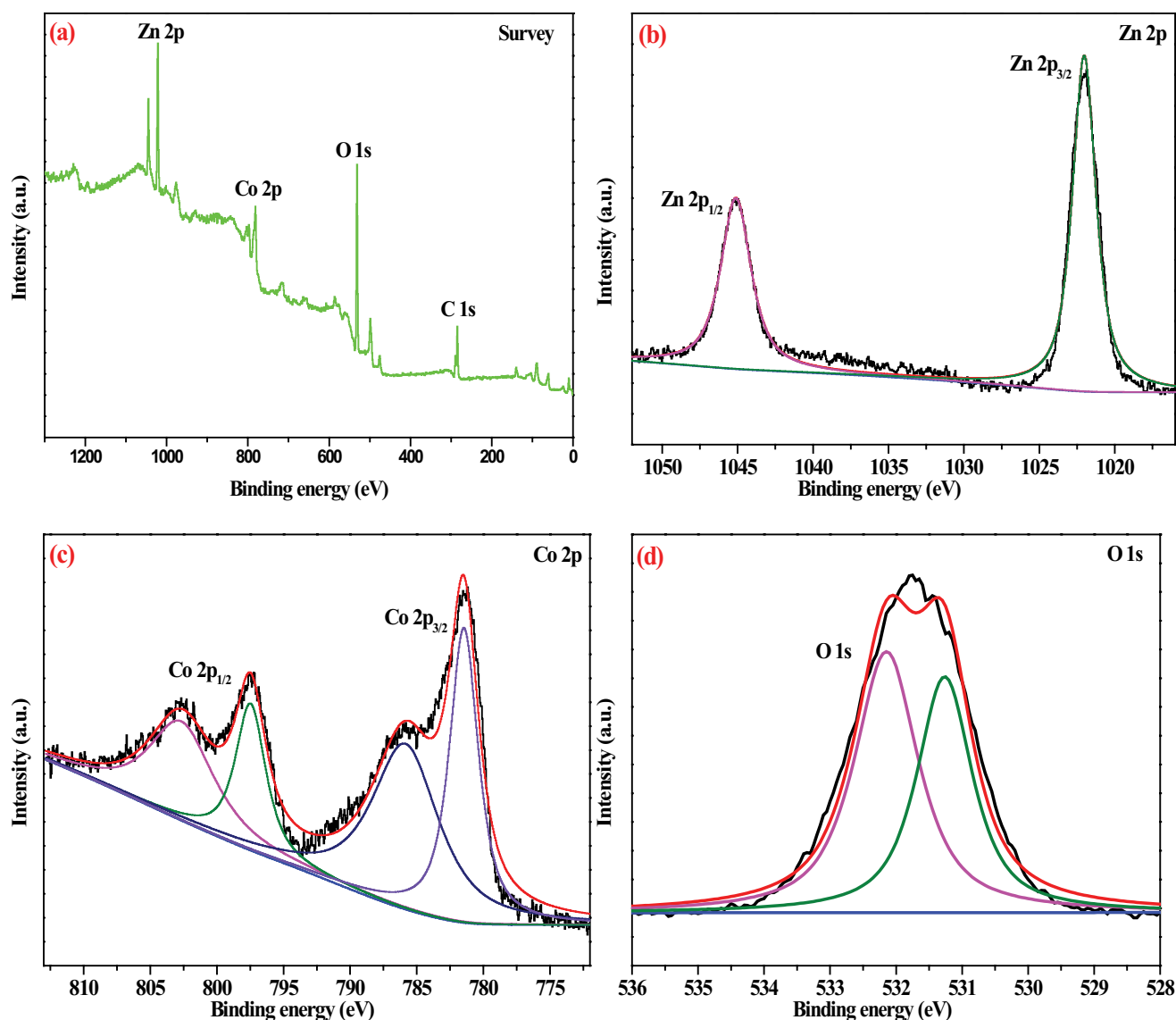
Fig. 4. XPS spectra of ZnCo-LDH (1:1): (a) the survey scans, (b) Zn 2p, (c) Co 2p, and (d) O 1s.

802.8 and 797.5 eV are assigned to the Co $2p_{1/2}$, and the binding energies of Co $2p_{3/2}$ shows two other peaks at 785.9 and 781.5 eV, which demonstrate the existence of the Co^{3+} and Co^{2+} oxidation states [30]. In addition, Fig. 4d shows that the binding energy of O1s and the strong peak located at 531.7 eV, which is attributed to the oxygen of the hydroxyl groups on the surface of the LDH [31]. The XPS results further confirm the successful formation of ZnCo-LDH.

3.2. Catalytic activity evaluation

3.2.1. Effect of different reaction system

As depicted in Fig. 5a, the degradation efficiency of RhB was explored by using different ZnCo-LDH samples in the ZnCo-LDH/PMS system. It was discovered that ZnAl-LDH as well as an unused catalyst cannot cause the degradation of RhB in dark. However, when the ZnCo-LDH samples were added, RhB can be oxidized and degraded by the generated various active species, which is owing to the effective activation of cobalt source for PMS. Among them, the optimal degradation efficiency of RhB was about 95% within 40 min in the ZnCo-LDH (1:1)/PMS dark process. Besides, the pseudo-first-order kinetics was used to evaluate the degradation performance of catalysts by using the general formulas ($\ln(C/C_0) = -kt$ and $t_{1/2} = \ln2/k$) where C/C_0 stands for the relative change of concentration, k (min^{-1}) is the pseudo-first-order rate constant and $t_{1/2}$ (min^{-1}) is half-life [32]. In Fig. 5b, the degradation process of RhB in dark was well accorded with the pseudo-first-order kinetics owing to which the correlation coefficients (R^2) are very close to 1. From Figs. 5c and d it can be seen that the highest rate is 0.0748 min^{-1}, and the shortest half-life is 8.89 min for the degradation of RhB in dark. The above experimental results revealed that 3D multi-layered ZnCo-LDH (1:1) catalyst can achieve better degradation of RhB due to which
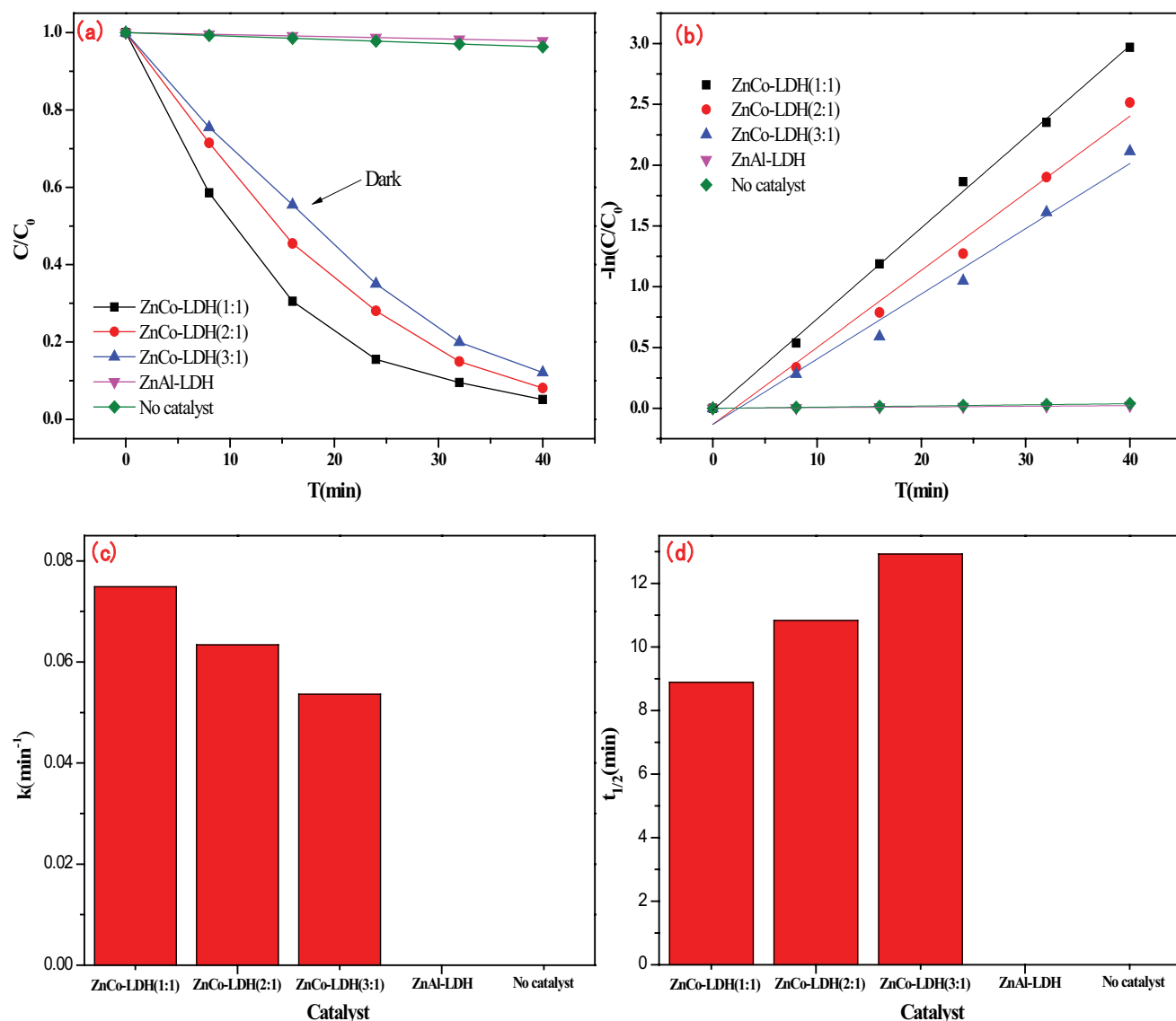
Fig. 5. (a–d) Degradation curve, pseudo-first-order kinetics model, reaction rate constants and half-lives of RhB with different catalysts in dark. (Experiment conditions: 10 mg L^{-1} RhB solution; 0.3 g L^{-1} PMS; 0.5 g L^{-1} catalyst; room temperature (25°C); no initial pH adjustment).

it provides a lots of cobalt-based active sites on the surface of multi-layered structure to enhance the activation of PMS.

In order to achieve the further enhancement of PMS activation, the ZnCo-LDH as an excellent cobalt-based catalyst can rapidly degrade RhB by various active species from activated PMS by introducing visible light irradiation. In Fig. 6a, ZnAl-LDH catalyst had weaker photocatalytical ability for the degradation of RhB. In addition, PMS cannot be completely activated under the condition of no catalyst, so the removal of RhB can only relied on itself weak activation of PMS. Compared with other several catalysts, the ZnCo-LDH (1:1) catalyst can achieve the complete degradation for RhB within 30 min. As shown in Fig. 6b, the degradation process of RhB was also accorded with the pseudo-first-order kinetics. From Figs. 6c and d, the ZnCo-LDH (1:1)/PMS system under visible light showed that the reaction rate (0.1008 min^{-1}) was faster more than that of

dark condition, and the half-life (6.87 min) is shorter. All the above results indicated that the combination of LDH catalyst with PMS can also further enhance the effective degradation of RhB by the assistance of visible light irradiation. Therefore, the 3D multi-layered ZnCo-LDH (1:1) material can be considered as a green and effective heterogeneous photoactivator in the ZnCo-LDH/PMS photosystem.

3.2.2. Effect of different anions

Some inorganic anions in the natural groundwater can cause an influence on the degradation reaction of RhB solution, such as Cl^-, NO_3^-, SO_4^{2-}, and HCO_3^-. In Fig. 7a, when 10 mM Cl^- was added, the degradation efficiency of RhB notably increased within 30 min. However, compared with existence of Cl^-, other three anions inhibited the generation of the $^\bullet OH$ and $SO_4^{\bullet-}$ radicals, which results in the decline
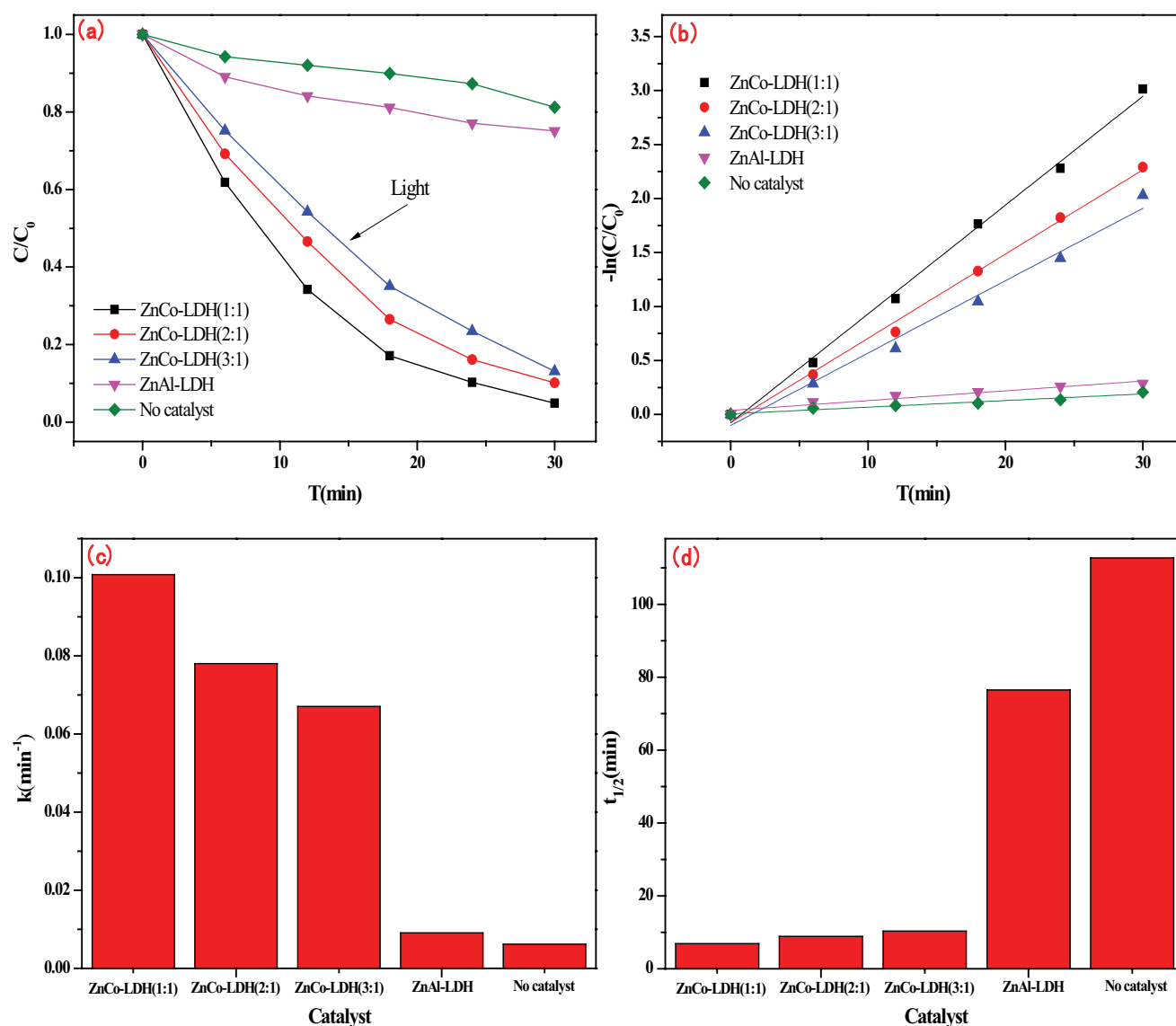
Fig. 6. (a–d) Degradation curve, pseudo-first-order kinetics model, reaction rate constants and half-lives of RhB with different catalysts under visible light. (Experiment conditions: 10 mg L⁻¹ RhB solution; 0.3 g L⁻¹ PMS; 0.5 g L⁻¹ catalyst; room temperature (25°C); no initial pH adjustment).

of RhB degradation efficiency. More specifically, when the reaction solution was, respectively, added an equal amount of NO_3^-, SO_4^{2-}, and HCO_3^-, RhB could be degraded to 91.4%, 92%, and 92.5% at the same time. As seen from Fig. 7b, the highest rate is 0.1151 min⁻¹ with the addition of Cl^-, but the reaction rates of solution with the other three anions were 0.0799, 0.082, and 0.087 min⁻¹, respectively. Therefore, it is necessary that the effect of the competitive adsorption of anions on the degradation processes of RhB should be clearly investigated.

Based on the above results and previous literatures, it was discovered that these inorganic anions were easily oxidized by $^\bullet OH$ and $SO_4^{\bullet-}$ radicals for a negative influence of RhB degradation efficiency, which is presented in these equations (Eqs. (1)–(9)) [33–36]. Obviously, the presence of Cl^- can enhance the degradation rate of RhB in the

ZnCo-LDH/PMS photosystem, which is ascribed to these three radicals including $Cl^\bullet$, $ClOH^{\bullet-}$, and $Cl_2^{\bullet-}$, respectively. Conversely, other three anions can decline the degradation rate of RhB, because the $^\bullet OH$ and $SO_4^{\bullet-}$ radicals can be easily quenched by these anions, which resulted in the generation of competitive relations with the target pollutions. In addition, it can be seen from Fig. 7b that the inhibiting order of these anions was $NO_3^- > SO_4^{2-} > HCO_3^-$. The above researches verified that the competitive adsorption of inorganic anions was largely responsible for the degradation rate of RhB:

$$Cl^- + {}^\bullet OH \rightarrow ClOH^{\bullet-} \tag{1}$$

$$ClOH^{\bullet-} + H^+ \rightarrow Cl^\bullet + H_2O \tag{2}$$
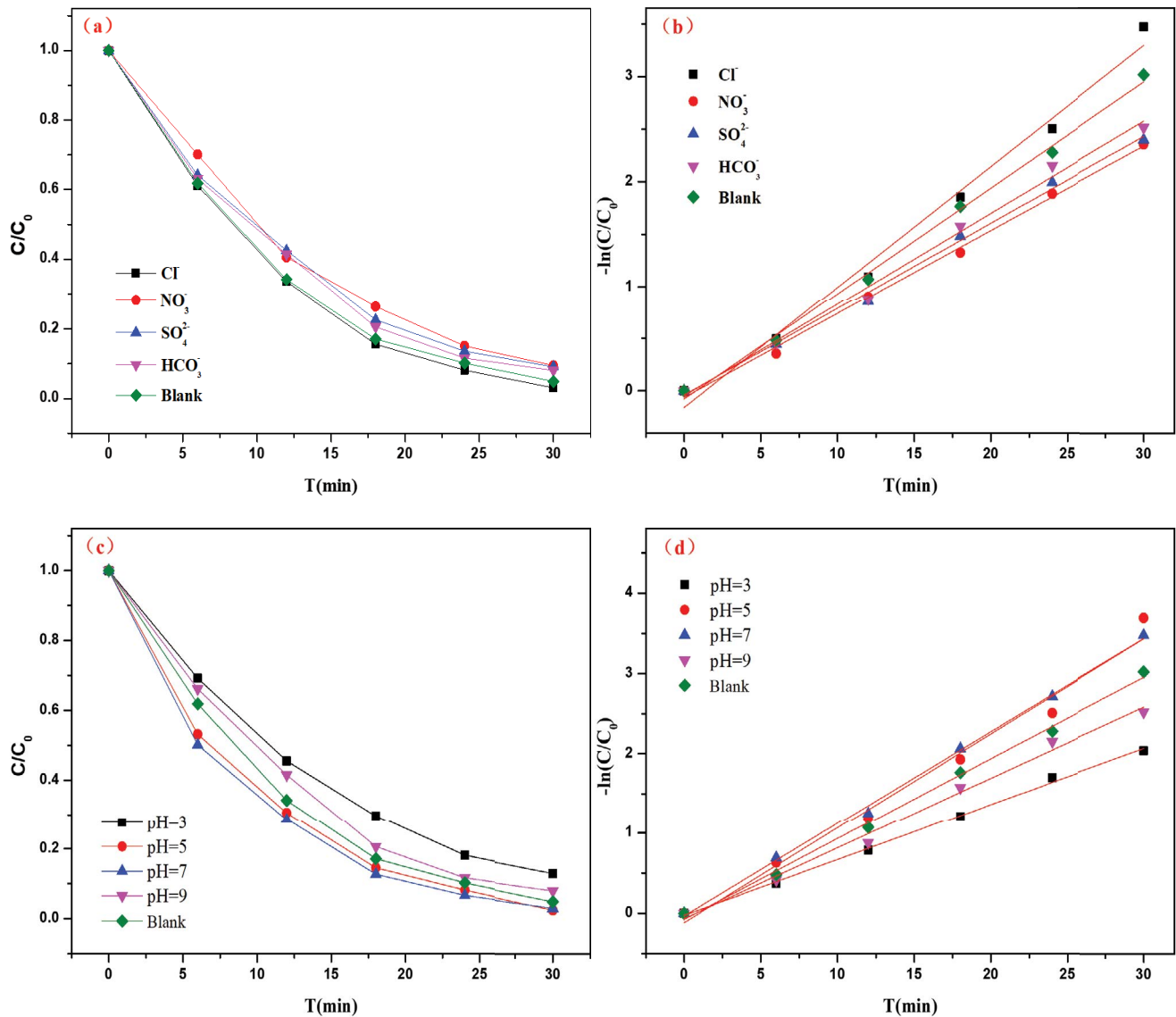
Fig. 7. (a–d) Degradation curve and pseudo-first-order kinetics model with different inorganic anions (pH values) under visible light. (Experiment conditions: 10 mg L^{-1} RhB solution; 0.3 g L^{-1} PMS; 0.5 g L^{-1} catalyst; room temperature (25°C)).

$$Cl^{\bullet} + Cl^{-} \rightarrow Cl_2^{\bullet-} \tag{3}$$

$$Cl^{-} + SO_4^{\bullet-} \rightarrow SO_4^{2-} + Cl^{\bullet} \tag{4}$$

$$NO_3^{-} + SO_4^{\bullet-} \rightarrow SO_4^{2-} + {}^{\bullet}NO_2 \tag{5}$$

$$NO_3^{-} + {}^{\bullet}OH \rightarrow OH^{-} + {}^{\bullet}NO_2 \tag{6}$$

$$SO_4^{2-} + {}^{\bullet}OH \rightarrow SO_4^{\bullet-} + OH^{-} \tag{7}$$

$$HCO_3^{-} + SO_4^{\bullet-} \rightarrow SO_4^{2-} + H^{+} + CO_3^{\bullet-} \tag{8}$$

$$HCO_3^{-} + {}^{\bullet}OH \rightarrow H_2O + CO_3^{\bullet-} \tag{9}$$

3.2.3. Effect of different pH

As shown in Fig. 7c, the effect of initial pH on the degradation efficiency of RhB was investigated at various pH conditions from 3 to 9. It was found that the degradation efficiency of RhB was more than 95% at the range of initial pH 4 to 7, so this PMS-AOPs synergistic techniques can be applied for the treatment of organic pollutants without pH adjustment. In addition, the higher catalytical activities were shown at pH ranging from 5 to 9 than extreme pH (pH = 3 or 9) in the ZnCo-LDH/PMS photosystem. Meanwhile, it is also observed from Fig. 7d that the reaction rate constants were 0.0695 min^{-1} (pH = 3), 0.118 min^{-1} (pH = 5), 0.115 min^{-1} (pH = 7), 0.088 min^{-1} (pH = 9), and 0.115 min^{-1} (blank group pH = 5.7), respectively. Compared with blank groups, the above results indicated that the degradation reaction of RhB was negative under extremely

acidic or alkaline conditions. On the one hand, an excess of H^+ could cause the loss of Co^{2+} from ZnCo-LDH catalyst for the negative effect on heterogeneous activation of PMS. On the other hand, it was also obvious that the degradation of RhB could be inhibited at extreme acidic or alkaline conditions, which presented in the following reactions (Eqs. (10)–(11)) [37,38]:

$$SO_5^{\bullet -} + H^+ \rightarrow HSO_5^{\bullet -} \tag{10}$$

$$SO_4^{\bullet -} + OH^- \rightarrow SO_4^{2-} + {}^{\bullet}OH \tag{11}$$

3.3. Possible degradation mechanism

In order to analyze the degraded processes of RhB, the free radicals quenching experiment was carried out in the ZnCo-LDH/PMS system under visible light irradiation. Typically, heterogeneous ZnCo-LDH/PMS system can generate two basical active species including ${}^{\bullet}OH$ and $SO_4^{\bullet -}$ radicals from the activation of PMS. According to previous reports, EtOH was found to have high reactivity for the quenching of ${}^{\bullet}OH$ radicals (reaction rate constant: $1.2–2.8 \times 10^9$ M^{-1} s^{-1}) and $SO_4^{\bullet -}$ radicals ($1.6–7.7 \times 10^7$ M^{-1} s^{-1}) [23]. Besides, TBA is more effective quenching for ${}^{\bullet}OH$ radicals ($3.87.6 \times 10^8$ M^{-1} s^{-1}) which is 1,000 times faster than $SO_4^{\bullet -}$ radicals ($4–9.1 \times 10^5$ M^{-1} s^{-1}) [39]. In view of the above analysis, EtOH (ethanol) is used to quench ${}^{\bullet}OH$ and $SO_4^{\bullet -}$ radicals, but TBA (*tert*-butyl alcohol) can only quench ${}^{\bullet}OH$ radicals. In Fig. 8a, when 0.2 mol L^{-1} TBA and EtOH were added into this system, the degradation efficiency of RhB declined to about 80% and 27%, respectively. Therefore, it can be seen that many $SO_4^{\bullet -}$ radicals and few ${}^{\bullet}OH$ radicals play an important role in the degradation processes of RhB.
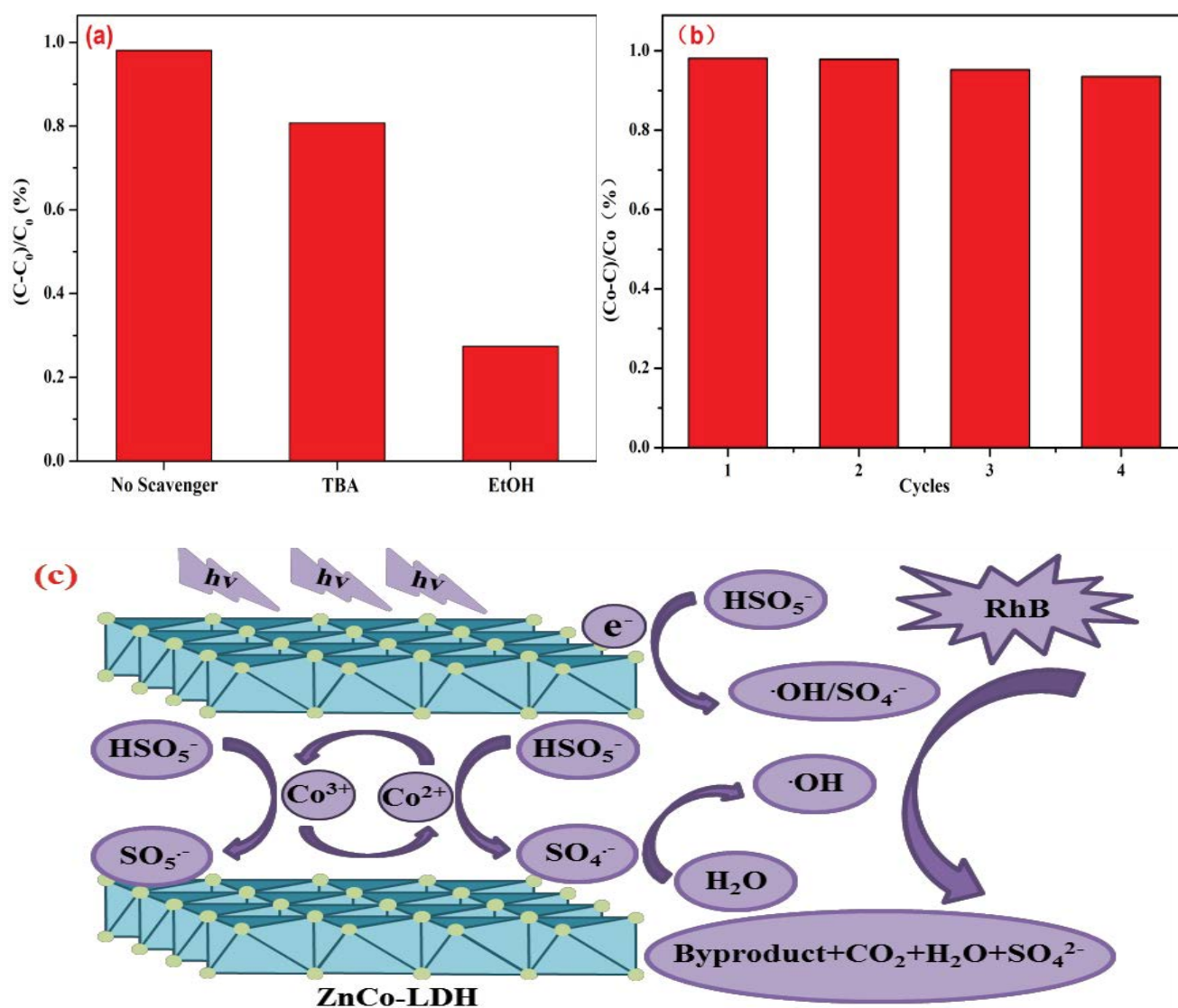
Fig. 8. (a) Effect of various radical scavengers on RhB degradation, (b) recycle test of ZnCo-LDH (1:1) for RhB degradation, and (c) Mechanism scheme for RhB degradation.

Based on above results, the possible mechanisms of ZnCo-LDH catalyst for the RhB degradation is proposed in Fig. 8c. In a typical photocatalytical reaction, ZnCo-LDH catalyst can be excited and produce the photo-generated electro–hole pairs in the conduction band under visible light irradiation. On the surface of catalyst, the photo-generated electrons (e^-) can react with the dissolved oxygen to produce the superoxide species ($^•O_2^-$), the photo-generated react holes (h^+) with water molecules to generate active $^•OH$ species (Eqs. (12)–(14)) [40,41]. Finally, small amount of RhB dye molecules can be oxidized and degraded by active $^•OH$ and $^•O_2^-$ species in the typical photocatalytic reaction (Eq. (15)) as follows:

$$ZnCo - LDH + hv \rightarrow LDH(e^-) + LDH(h^+) \tag{12}$$

$$LDH(e^-) + O_2 \rightarrow LDH + {^•O_2^-} \tag{13}$$

$$LDH(h^+) + H_2O \rightarrow LDH + {^•OH} \tag{14}$$

$${^•O_2^-} + {^•OH} + RhB \rightarrow By\text{-}products + H_2O + CO_2 \tag{15}$$
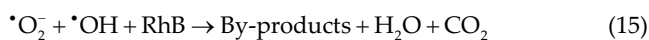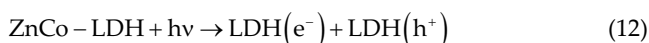
In addition, PMS-AOPs technology plays a major role for the degradation of RhB. Firstly, the photo-generated electrons can react with HSO_5^- from PMS to produce $SO_4^{•-}$ species (Eq. (16)) [41]. On the other hand, Co^{2+} can be activated by HSO_5^- and generate $SO_4^{•-}$ species, and Co^{3+} can also be captured and generate $SO_5^{•-}$ species (Eqs. (17) and (18)) [42,43]. Further, main $^•OH$ species were obtained by $SO_4^{•-}$ species reacting with water molecules, and $SO_4^{•-}$ species can also obtained by its own oxidation reaction of $SO_5^{•-}$ species (Eq. (19) and (20)) [44,45]. Lastly, the generated $SO_4^{•-}$ and $^•OH$ radicals can effectively oxidate RhB dye molecules to achieve complete degradation (Eq. (21)). Briefly, PMS can be heterogeneously activated by the synergetic assistance of the photo-induced electrons and cobalt source, and then the relevant reactions for PMS activation by the ZnCo-LDH/PMS photosystem were shown as follows:

$$HSO_5^- + LDH(e^-) \rightarrow OH^- + SO_4^{•-} \tag{16}$$

$$Co^{2+} + HSO_5^- \rightarrow Co^{3+} + SO_4^{•-} + {^•OH} \tag{17}$$

$$Co^{3+} + HSO_5^- \rightarrow Co^{2+} + SO_5^{•-} + H^+ \tag{18}$$

$$SO_4^{•-} + H_2O \rightarrow H^+ + SO_4^{2-} + {^•OH} \tag{19}$$

$$SO_5^{•-} + SO_5^{•-} \rightarrow O_2 + 2SO_4^{•-} \tag{20}$$

$$SO_4^{•-} + {^•OH} + RhB \rightarrow By\text{-}products + SO_4^{2-} + H_2O + CO_2 \tag{21}$$
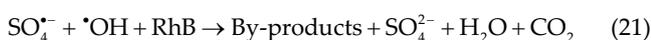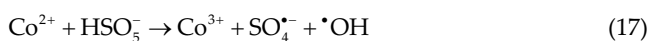
3.4. Reusability of the catalyst

The stability evaluations of the catalyst are widely concerned for their practical applications. In this system, the sustainable reusability of ZnCo-LDH (1:1) catalyst was estimated by the cycle experiment. Specifically, the used catalysts were collected by centrifugation, then washing with ethanol and deionized water for several times, and dried at 60°C for the next utilization. As shown in Fig. 8b, the degradation efficiency of RhB can still keep over 95% after four continual cycles, which indicated that the ZnCo-LDH catalyst has excellent stability and reusability for the degradation of refractory pollutants from wastewater.

4. Conclusion

In this study, 3D multi-layered ZnCo-LDH, prepared via the facile one-step hydrothermal method, was used for the first time as heterogeneous photoactivator which has good crystallographic structure and large surface area to offer more active site. Therefore, ZnCo-LDH can photoactivate PMS to achieve the highly efficient degradation of RhB under visible light irradiation, and the reaction processes were accorded well with the pseudo-first-order kinetic behaviors. In the ZnCo-LDH/PMS photosystem, the synergetic action of the photo-induced electrons and cobalt cations play a major role in the degradation of RhB. Briefly, this work could provide a simple idea to fabricate novel cobalt-based catalyst with high catalytical activity and excellent stability for all kinds of applications in the treatment of organic pollutants.

References

[1] S.Y. Janbandhu, A. Joshi, S.R. Munishwar, R.S. Gedam, CdS/TiO$_2$ heterojunction in glass matrix: synthesis, characterization, and application as an improved photocatalyst, Appl. Surf. Sci., 497 (2019) 143758, doi: 10.1016/j.apsusc.2019.143758.

[2] G. Salehi, R. Abazari, A.R. Mahjoub, Visible-light-induced graphitic-C$_3$N$_4$@nickel-aluminum layered double hydroxide nanocomposites with enhanced photocatalytic activity for removal of dyes in water, Inorg. Chem., 57 (2018) 8681–8691.

[3] Z.J. Zhang, Y. Yang, L. Sun, R. Liu, Direct conversion of metal- polyphenolic coordination assembly to MnO$_x$-carbon nanocomposites for catalytic degradation of methylene blue, Mater. Lett., 221 (2018) 97–100.

[4] J. Qiao, H.B. Zhang, G.S. Li, S.Y. Li, Z.H. Qu, M. Zhang, J. Wang, Y.T. Song, Fabrication of a novel Z-scheme SrTiO$_3$/Ag$_2$S/CoWO$_4$ composite and its application in sonocatalytic degradation of tetracyclines, Sep. Purif. Technol., 211 (2019) 843–856.

[5] A. Khataee, S.A. Oskoui, L. Samaei, ZnFe-Cl nanolayered double hydroxide as a novel catalyst for sonocatalytic degradation of an organic dye, Ultrason. Sonochem., 40 (2018) 703–713.

[6] X. Cao, H. Wang, S. Zhang, O. Nishimura, X.N. Li, Azo dye degradation pathway and bacterial community structure in biofilm electrode reactors, Chemosphere, 208 (2018) 219–225.

[7] M. Xu, B. Bi, B.B. Xu, Z.X. Sun, L. Xu, Polyoxometalate-intercalated ZnAlFe-layered double hydroxides for adsorbing removal and photocatalytic degradation of cationic dye, Appl. Clay Sci., 157 (2018) 86–91.

[8] F. Ghanbari, M. Moradi, Application of peroxymonosulfate and its activation methods for degradation of environmental organic pollutants: review, Chem. Eng. J., 102 (2017) 307–315.

[9] H.X. Li, S.D. Xu, J. Du, J.H. Tang, Q.W. Zhou, Cu@Co-MOFs as a novel catalyst of peroxymonosulfate for the efficient removal of methylene blue, RSC Adv., 9 (2019) 9410–9420.

[10] A. Shahzad, A. Jawad, J. Ifthikar, Z.L. Chen, Z.Q. Chen, The hetero-assembly of reduced graphene oxide and hydroxide nanosheets as superlattice materials in PMS activation, Carbon, 155 (2019) 740–755.

[11] X.Q. Chen, M. Murugananthan, Y.R. Zhang, Degradation of p-Nitrophenol by thermally activated persulfate in soil system, Chem. Eng. J., 283 (2017) 1357–1365.

[12] Y.X. Liu, Y. Wang, Gaseous elemental mercury removal using combined metal ions and heat activated peroxymonosulfate/ H_2O_2 solutions, AICHE J., 1 (2019) 161–174.

[13] P.D. Hu, M.C. Long, Cobalt-catalyzed sulfate radical-based advanced oxidation: a review on heterogeneous catalysts and applications, Appl. Catal., B, 181 (2016) 103–117.

[14] M. Xie, J.C. Tang, L.S. Kong, W.H. Lu, V. Natarajan, F. Zhu, J.H. Zhan, Cobalt doped g-C$_3$N$_4$ activation of peroxymonosulfate for monochlorophenols degradation, Chem. Eng. J., 360 (2019) 1213–1222.

[15] T. Zeng, X.L. Zhang, S.H. Wang, H.Y. Niu, Y.Q. Cai, Spatial confinement of a Co$_3$O$_4$ catalyst in hollow metal-organic frameworks as a nanoreactor for improved degradation of organic pollutants, Environ. Sci. Technol., 4 (2015) 2350–2357.

[16] T. Li, J. Wang, Y. Xu, Y.D. Cao, H.Z. Lin, T. Zhang, Hierarchical structure formation and effect mechanism of Ni/Mn layered double hydroxides microspheres with large-scale production for flexible asymmetric supercapacitors, ACS Appl. Energy Mater., 1 (2018) 2242–2253.

[17] G.Q. Zhao, C.F. Li, X. Wu, J.G. Yu, X.Y. Jiang, W.J.H. Hu, Reduced graphene oxide modified NiFe-calcinated layered double hydroxides for enhanced photocatalytic removal of methylene blue, Appl. Surf. Sci., 434 (2018) 251–259.

[18] L.N. Dang, H.F. Liang, J.Q. Zhuo, B.K. Lamb, H.Y. Sheng, Y. Yang, S. Jin, Direct synthesis and anion exchange of noncarbonate-intercalated NiFe-layered double hydroxides and the influence on electrocatalysis, Chem. Mater., 30 (2018) 4321–4330.

[19] X.W. Lv, X. Xiao, M.L. Cao, Y. Bu, C.Q. Wang, M.K. Wang, Y. Shen, Efficient carbon dots/NiFe-layered double hydroxide/ BiVO$_4$ photoanodes for photoelectrochemical water splitting, Appl. Surf. Sci., 439 (2018) 1065–1071.

[20] J.F. Yu, Q. Wang, D. O'Hare, L.Y. Sun, Preparation of two dimensional layered double hydroxide nanosheets and their applications, Chem. Soc. Rev., 46 (2017) 5950–5974.

[21] S. Zhou, C.F. Li, G.Q. Zhao, L.K. Liu, J.G. Yu, X.Y. Jiang, F.P. Jiao, Heterogeneous co-activation of peroxymonosulfate by CuCoFe calcined layered double hydroxides and ultraviolet irradiation for the efficient removal of p-nitrophenol, J. Mater. Sci.: Mater. Electron., 30 (2019) 19009–19019.

[22] E.M. Seftel, M. Puscasu, M. Mertens, P. Cool, G. Carja, Photoresponsive behavior of γ-Fe$_2$O$_3$ NPs embedded into ZnAlFe-LDH matrices and their catalytic efficiency in waste-water remediation, Catal. Today, 252 (2015) 7–13.

[23] M. Li, L.M. Farmen, C.K. Chan, Selenium removal from sulfate- containing groundwater using granular layered double hydroxide materials, Ind. Eng. Chem. Res., 56 (2017) 2458–2465.

[24] X.F. Zhao, C.G. Niu, L. Zhang, H. Guo, X.J. Wen, C. Liang, G.M. Zeng, Co-Mn layered double hydroxide as an effective heterogeneous catalyst for degradation of organic dyes by activation of peroxymonosulfate, Chemosphere, 204 (2018) 11–21.

[25] A. Mantilla, F. Tzompantzi, J.L. Fernández, J.A.I. Díaz Góngora, G. Mendoza, R. Gómez, Photodegradation of 2,4-dichlorophenoxyacetic acid using ZnAlFe layered double hydroxides as photocatalysts, Catal. Today, 148 (2019) 119–123.

[26] Z.W. Wu, H.Z. Zhang, L.L. Luo, W.X. Tu, ZnCo binary hydroxide nanostructures for the efficient removal of cationic dyes, J. Alloys Compd., 806 (2019) 823–832.

[27] Y. Lu, B. Jiang, L. Fang, F.L. Ling, J.M. Gao, F. Wu, X.H. Zhang, High performance NiFe layered double hydroxide for methyl orange dye and Cr(VI) adsorption, Chemosphere, 152 (2016) 415–422.

[28] L.G. Yan, K. Yang, R.R. Shan, T. Yan, J. Wei, S.J. Yu, H.Q. Yu, B. Du, Kinetic, isotherm and thermodynamic investigations of phosphate adsorption onto core-shell Fe$_3$O$_4$@LDHs composites

with easy magnetic separation assistance, J. Colloid Interface Sci., 448 (2015) 508–516.

[29] Y. Li, L. Zhang, X. Xiang, D.P. Yan, F. Li, Engineering of ZnCo-layered double hydroxide nanowalls toward high-efficiency electrochemical water oxidation, J. Mater. Chem. A, 2 (2014) 13250–13258.

[30] J.J. Zhou, X. Han, K. Tao, Q. Li, Y.L. Li, C. Chen, L. Han, Shish-kebab type MnCo$_2$O$_4$@Co$_3$O$_4$ nanoneedle arrays derived from MnCoLDH@ZIF-67 for high-performance supercapacitors and efficient oxygen evolution reaction, Chem. Eng. J., 354 (2018) 875–884.

[31] H.L. Zhou, Y.X. Song, Y.C. Liu, H.D. Li, W.J. Li, Z.D. Chang, Fabrication of CdS/Ni-Fe LDH heterostructure for improved photocatalytic hydrogen evolution from aqueous methanol solution, Int. J. Hydrogen Energy, 43 (2018) 14328–14336.

[32] G.Q. Zhao, D. Zhang, J.G. Yu, Y. Xie, W.J.H. Hu, F.P. Jiao, Multi-walled carbon nanotubes modified Bi$_2$S$_3$ microspheres for enhanced photocatalytic decomposition efficiency, Ceram. Int., 43 (2017) 15080–15088.

[33] P. Wang, S.Y. Yang, L. Shan, R. Niu, X.T. Shao, Involvements of chloride ion in decolorization of Acid Orange 7 by activated peroxydisulfate or peroxymonosulfate oxidation, J. Environ. Sci. China, 23 (2011) 1799–1807.

[34] Y.F. Ji, C.X. Dong, D.Y. Kong, J.K. Lu, New insights into atrazine degradation by cobalt catalyzed peroxymonosulfate oxidation: kinetics, reaction products and transformation mechanisms, J. Hazard. Mater., 285 (2015) 491–500.

[35] Z.Y. Shen, H.Y. Zhou, Z.C. Pan, Y. Guo, Y. Yuan, G. Yao, B. Lai, Degradation of atrazine by Bi$_2$MoO$_6$ activated peroxymonosulfate under visible light irradiation, J. Hazard. Mater., 400 (2020) 123187, doi: 10.1016/j.jhazmat.2020.123187.

[36] Z.L. Wu, Y.P. Wang, Z.K. Xiong, Z.M. Ao, S.Y. Pu, G. Yao, B. Lai, Core-shell magnetic Fe$_3$O$_4$@Zn/Co-ZIFs to activate peroxymonosulfate for highly efficient degradation of carbamazepine, Appl. Catal., B, 277 (2020) 119136, doi: 10.1016/j.apcatb.2020.119136.

[37] J.C. Yana, Y. Chen, L.B. Qian, W.G. Gao, D. Ouyang, M.F. Chen, Heterogeneously catalyzed persulfate with a CuMgFe layered double hydroxide for the degradation of ethylbenzene, J. Hazard. Mater., 338 (2017) 372–380.

[38] T. Zhang, H. Zhu, J.P. Croue, Production of sulfate radical from peroxymonosulfate induced by a magnetically separable CuFe$_2$O$_4$ spinel in water: efficiency, stability, and mechanism, Environ. Sci. Technol., 47 (2013) 2784–2791.

[39] N. Jaafarzadeh, F. Ghanbari, M. Ahmadi, Catalytic degradation of 2,4-dichlorophenoxyacetic acid (2,4-D) by nano-Fe$_2$O$_3$ activated peroxymonosulfate: influential factors and mechanism determination, Chemosphere, 169 (2017) 568–576.

[40] Y.Y. Chen, X. Xie, Y.S. Si, P.Y. Wang, Q.S. Yan, Constructing a novel hierarchical β-Ag$_2$MoO$_4$/BiVO$_4$ photocatalyst with Z-scheme heterojunction utilizing Ag as an electron mediator, Appl. Surf. Sci., 498 (2019) 143860, doi: 10.1016/j.apsusc.2019.143860.

[41] G.Q. Zhao, J. Zou, C.F. Li, J.G. Yu, X.Y. Jiang, Y.J. Zheng, W.J.H. Hu, F.P. Jiao, Enhanced photocatalytic degradation of rhodamine B, methylene blue and 4-nitrophenol under visible light irradiation using TiO$_2$/MgZnAl layered double hydroxide, J. Mater. Sci., 29 (2018) 7002–7014.

[42] M.F. Ma, L. Chen, J.Z. Zhao, W. Liu, H.D. Ji, Efficient activation of peroxymonosulfate by hollow cobalt hydroxide for degradation of ibuprofen and theoretical study, Chin. Chem. Lett., 30 (2019) 2191–2195.

[43] A. Khana, Z.W. Liao, Y. Liu, A. Jawad, J. Ifthikar, Z.Q. Chen, Synergistic degradation of phenols using peroxymonosulfate activated by CuO-Co$_3$O$_4$@MnO$_2$ nanocatalyst, J. Hazard. Mater., 329 (2017) 262–271.

[44] Y. Zhou, X. Wang, C. Zhu, D.D. Dionysiou, G. Zhao, G. Fang, D. Zhou, New insight into the mechanism of peroxymonosulfate activation by sulfur-containing minerals: role of sulfur conversion in sulfate radical generation, Water Res., 142 (2018) 208–216.

[45] C. Lyu, D. He, Z.S. Mou, X.J. Yang, Synergetic activation of peroxymonosulfate by MnO$_2$-loaded β-FeOOH catalyst for enhanced degradation of organic pollutant in water, Sci. Total Environ., 693 (2019) 133589, doi: 10.1016/j.scitotenv.2019.133589.